Research Paper

Chemotherapy priming of the Pancreatic Tumor Microenvironment Promotes Delivery and Anti-Metastasis Efficacy of Intravenous Low-Molecular-Weight Heparin-Coated Lipid-siRNA Complex

Qianwen Yu, Yue Qiu, Xiaoxiao Chen, Xuhui Wang, Ling Mei, Haiyao Wu, Kai Liu, Yayuan Liu, Man Li, Zhirong Zhang, Qin He✉

Key Laboratory of Drug Targeting and Drug Delivery Systems, West China School of Pharmacy, Sichuan University, No. 17, Block 3, Southern Renmin Road, Chengdu 610041, China

✉ Corresponding author: Qin He, Key Laboratory of Drug Targeting and Drug Delivery Systems, West China School of Pharmacy, Sichuan University, No. 17, Block 3, Southern Renmin Road, Chengdu 610041, China. E-mail addresses: qinhe@scu.edu.cn; Tel/Fax: +86-028-85502532.

Abstract

Pancreatic ductal adenocarcinoma (PDAC) is a type of malignant tumor with high lethality. Its high tumor cell-density and large variety of extracellular matrix (ECM) components present major barriers for drug delivery.

Methods: Paclitaxel-loaded PEGylated liposomes (PTX-Lip) were used as a tumor-priming agent to induce tumor cell apoptosis and decrease the abundance of ECM to promote cellular uptake and tumor delivery of nanodrugs. Paclitaxel exerts anti-cancer effects but, paradoxically, exacerbates cancer metastasis and drug resistance by increasing the expression of apoptotic B-cell lymphoma-2 protein (BCL-2). Thus, low-molecular-weight heparin-coated lipid-siRNA complex (LH-Lip/siBCL-2) was constructed to inhibit cancer metastasis and silence BCL-2 by BCL-2 siRNA (siBCL-2).

Results: Significant tumor growth inhibition efficacy was observed, accompanied by obvious inhibition of cancer metastasis *in vivo*.

Conclusion: These results suggested our sequential delivery of PTX-Lip and LH-Lip/siBCL-2 might provide a practical approach for PDAC or other ECM-rich tumors.

Key words: pancreatic cancer, tumor priming, low-molecular-weight heparin, chemo-gene therapy, metastasis

Introduction

Pancreatic ductal adenocarcinoma (PDAC), also known as pancreatic cancer, is a type of malignant tumor with high lethality and a low survival rate [1]. Compared to other solid tumors, pancreatic tumors always contain a large variety of extracellular matrix (ECM) components such as collagen I, hyaluronic acids and cancer-associated fibroblasts, which are associated with the development and metastasis of cancer. Moreover, ECM increases tumor stroma pressure. The dense stroma forms a physical barrier that makes nanocarriers more difficult to deliver [2].

Previous studies have shown that the rate and extent of penetration of small-molecule drugs or nanocarriers into solid tumors is related to the composition and structure of the tumor tissue and the density of the tumor cells [3]. Tumor priming is an emerging strategy that reduces the density of tumor cells using chemotherapeutics, and promotes the delivery and efficacy of nanodrugs in solid tumors [4]. However, chemotherapy is a double-edged sword:

paradoxically, paclitaxel (PTX) kills cancer cells to exert anti-cancer effects but exacerbates cancer metastasis. Yi et al. demonstrated that PTX improves the tumor microenvironment for cancer cells to metastasize via Atf3 gene, a stress-inducible gene [5]. Furthermore, chemotherapy can cause serious side effects because of its cytotoxicity to normal tissues following systemic administration.

In our study, paclitaxel-loaded PEGylated liposomes (PTX-Lip) at a low dosage were used as a tumor-priming agent to enhance the delivery of nanocarriers into pancreatic tumors. PTX-Lip was used to instead of free PTX, which was used as the tumor-priming agent in a previous study [6]. In this study, a low dose of PTX-Lip (50 mg/m^2) significantly reduced myelosuppression and hepatotoxicity compared to free PTX (100 mg/m^2) but exerted a similar effect for tumor priming. Furthermore, PTX-Lip regulated the tumor microenvironment by inducing tumor cell apoptosis and decreasing interstitial fibrosis of the tumor.

In order to further minimize the negative factors of drug resistance and cancer metastasis caused by chemotherapeutics, we further constructed low-molecular-weight heparin-coated cationic liposomes (LH-Lip) carrying B-cell lymphoma-2 protein siRNA (LH-Lip/siBCL-2), which were administered following low dose pretreatment with PTX-Lip. B-cell lymphoma-2 protein (BCL-2) is an important regulatory protein in the apoptosis pathway that promotes cell survival mainly by inhibiting cell apoptosis [7]. Most chemotherapeutics including PTX and doxorubicin can trigger the apoptosis pathway and activate a cellular defense mechanism of anti-apoptosis by increasing the expression of BCL-2, which prevents cell death and induces drug resistance [8]. Moreover, emerging evidence has revealed that BCL-2 family proteins are regulators associated with cancer cell invasion and metastasis, and BCL-2 expression levels are positively correlated with cancer metastasis [9]. Therefore, BCL-2 siRNA (siBCL-2) was chosen to silence the BCL-2 expression of pancreatic cancer cells for cancer therapy.

In designing LH-Lip/siBCL-2, cationic liposomes were coated with low-molecular-weight heparin to reduce their toxicity and enhance anti-metastasis efficacy. Cationic liposomes are widely used in gene delivery as they are biodegradable due to their biological membranous structure and exhibit lower immunogenicity and toxicity compared to viral carriers [10]. However, they may cause potential toxicity both *in vitro* and *in vivo*. Wei et al. demonstrated that cationic liposomes induced cell necrosis and caused a serious inflammatory response [11]. Introduction of excessively positively charged

nanoparticles into systemic circulation causes hemolysis and embolism, and the nanoparticles adsorb various plasma proteins, resulting in nanoparticle aggregation [12]. Mucopolysaccharides, including hyaluronic acid, chondroitin sulfate, and heparin, constitute the main components of connective tissue. Researchers have found that encapsulating chondroitin sulfate on the surface of cationic carriers greatly reduces their toxicity and increases their stability [13]. Except chondroitin sulfate, low-molecular-weight heparin (LH) has been applied as a good alternative to unfractionated heparin with fewer side effects and exhibits potent anti-metastatic efficacy in nanoformulations [14]. The results of our study showed that LH-Lip played a major role in inhibiting cancer metastasis and prolonged the survival of tumor-bearing mice.

Here, we designed a novel dosing regimen that consists of a low dose pretreatment with PTX-Lip accompanied by sequential administration of LH-Lip/siBCL-2 (**Scheme 1**). In step 1, a low dose of PTX-Lip is used as a tumor-priming agent to regulate the tumor microenvironment and promote the delivery of nanodrugs. In step 2, LH-Lip/siBCL-2 is sequentially administrated to inhibit cancer metastasis and downregulate the expression of BCL-2. Anti-tumor and antimetastasis efficacies were evaluated both *in vitro* and *in vivo*.

Methods

Chemicals and reagents

Cholesterol was purchased from Chengdu Kelong Chemical Company (Chengdu, China). Soybean phospholipids (SPC) were purchased from Shanghai Taiwei Chemical Company (Shanghai, China). 1, 2-dioleoyl-3-trimethylammonium-propane (DOTAP) was obtained from Shanghai Advanced Vehicle Technology (AVT) Ltd. (Shanghai, China). DSPE-PEG2000-OMe and 1, 2-dioleoyl-sn-glycero-3-phosp-hoethanolamine-N-(carboxyfluorescein) (CFPE) were purchased from Avanti Polar Lipids (Alabaster, AL, USA). Protamine sulfate (fraction X from salmon) and calf thymus DNA were purchased from Sigma–Aldrich (St. Louis, MO, USA). Paclitaxel (PTX) and low-molecular-weight heparin (Enoxaparin sodium, LH) were purchased from Melonepharma (Dalian, China). BCL-2 siRNA, scrambled siRNA and Cy5-labeled siRNA were purchased from Gene Pharma Ltd. (Shanghai, China). The BCL-2 siRNA (siBCL-2) sense sequence is 5'-GUG AUG AAG UAC AUC CAU UdTdT-3', and the anti-sense sequence is 5'-AAU GGA UGU ACU UCA UCA CdTdT-3'. The scramble siRNA (siCTL) sense sequence is 5'-UUC UCC GAA CGU GUC ACG UTT-3', and the

anti-sense sequence is 5'-ACG UGA CAC GUU CGG AGA ATT-3'.

Preparation and characterization of lipid-siRNA complex (lipoplex)

Lipoplex was prepared using the thin film hydration method. 2.0 mg of cholesterol and 3.6 mg of DOTAP (molar ratio = 1:1) were dissolved in 1 mL of chloroform. Then, the organic solvent was evaporated by rotary evaporation under a vacuum, and the film was formed and hydrated in 1 mL DEPC (diethyl pyrocarbonate)-treated deionized water (ddH$_2$O) at 37 °C for 20 min and sonicated at 80 W for 100 s. siRNA-loaded naked cationic liposome complex (N-Lip/siRNA) was prepared by mixing equal volumes of suspension A (8.3 mM liposome and 200 mg/mL protamine) and suspension B (160 mg/mL siRNA and 160 mg/mL calf thymus DNA) and incubating for 10 min at room temperature. Then, N-Lip/siRNA was filtered using ultra-filtration tubes (30 kDa, Pall Corporation, Ann Arbor, Michigan, USA), and the free siRNA was removed by centrifugation at 9300 rcf for 30 min. Likewise, CFPE-labeled lipoplex was prepared by adding 400 µL of CFPE (100 µg/mL) to the organic solution before the lipid film was formed.
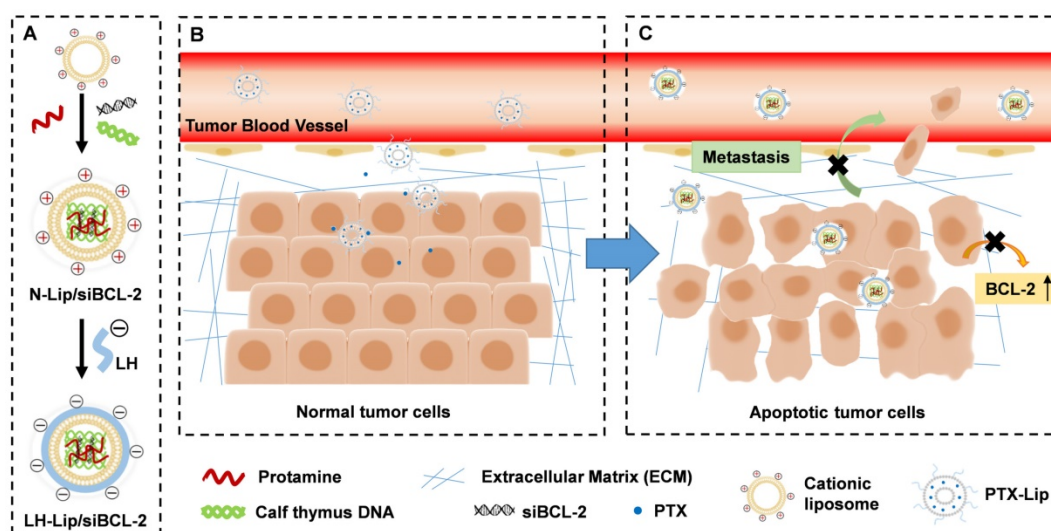
LH-Lip/siRNA was prepared by mixing N-Lip/siRNA with an equal volume of LH solution (0, 1, 2, 3, 4, 5, 6, 7, 8, 9, and 10 mg/mL, dissolved in ddH$_2$O). LH solution was added dropwise into N-Lip/siRNA (4 mM lipid) and then magnetically stirred for 10 min at room temperature. The hydrodynamic diameters and zeta potentials of lipoplexes were detected using a Malvern Zetasizer Nano ZS90 (Malvern Instruments Ltd., Malvern, UK). The morphology of LH-Lip/siBCL-2 was observed under a transmission electronic microscope (TEM; JEM 100CX, JEOL Ltd., Tokyo, Japan). The entrapment efficiency (EE) of siRNA was determined using Cy5-labeled siRNA as previously described [15]. The ability of N-Lip to form self-assembled complexes with siRNA was measured by agarose gel electrophoresis. N-Lip/siRNA at charge ratios N/P varying from 1/1 to 10/1 were prepared.

Cellular uptake

BXPC-3 cells were seeded on 6-well plates at a density of ~5×10^5 cells/well and incubated overnight. PTX-Lip was added at a final PTX concentration of 0.3 µg/mL. After 24 h, CFPE-labeled N-Lip/siBCL-2 and LH-Lip/siBCL-2 were added at a final CFPE concentration of 2 µg/mL. After 2 h, the cells were washed twice with phosphate buffered saline (PBS), and were trypsinized and resuspended in 0.3 mL PBS. The fluorescence intensity of cells was measured by flow cytometry (Cytomics™ FC 500, Beckman Coulter, Miami, FL, USA).

To evaluate the cellular uptake after priming with different concentrations of PTX, BXPC-3 cells were seeded and pretreated with PTX-Lip (0, 0.1, 0.3, 0.6, and 1 µg/mL PTX). After 24 h, CFPE-labeled LH-Lip/siBCL-2 was added as described above. The fluorescence intensity of cells was measured by flow cytometry (Cytomics™ FC 500, Beckman Coulter, Miami, FL, USA).

Scheme 1. Diagram of chemotherapy priming combined with low-molecular-weight heparin-coated lipid-siRNA complex (LH-Lip/siBCL-2) against pancreatic tumor and metastasis. **(A)** BCL-2 siRNA was encapsulated in cationic liposomes with the help of protamine and calf thymus DNA to form N-Lip/siBCL-2. Then, N-Lip/siBCL-2 was surface-coated with low-molecular-weight heparin to form LH-Lip/siBCL-2. **(B)** A low dose of PTX-Lip was administered as a tumor-priming agent to regulate the tumor microenvironment and promote the delivery of nanodrugs. **(C)** LH-Lip/siBCL-2 was sequentially administrated to inhibit cancer metastasis and downregulate the expression of BCL-2.

Silencing effect of siBCL-2-loaded lipoplex

BXPC-3 cells were seeded and pretreated with PTX-Lip (0, 0.1, 0.3, 0.6, and 1 µg/mL PTX) for 24 h as described above. Then, the cells were collected and washed twice using staining buffer (PBS containing 2% bovine serum albumin and 0.1% NaN_3). Next, the cells were incubated with FITC-labeled goat anti-rabbit BCL-2 antibody. After 1 h, the cells were washed and resuspended in 0.3 mL staining buffer for flow cytometry analysis (Cytomics™ FC 500, Beckman Coulter, Miami, FL, USA).

For the silencing study, formulations with siRNA (50 nM) were added after the incubation with PTX-Lip (0.3 µg/mL). After 24 h, the cells were processed as described above.

Tumor penetration

Tumor-bearing mice were randomized into 4 groups (6 mice/group): PBS, PTX-Lip (50 mg/m²), PTX-Lip (100 mg/m²), and free PTX (dissolved in ethanol-Cremophor ELP 35 mixture, v/v = 1:1,100 mg/m²). 24 h and 48 h after injection of the above formulations, mice were injected with DID-labeled LH-Lip. After 24 h, mice were euthanized via cardiac perfusion with PBS and 4% paraformaldehyde. The tumors were collected and imaged using the IVIS spectrum system (Caliper Life Sciences, Hopkinton, MA, USA) and cryosectioned at a thickness of 10 µm. The sections were firstly stained with primary anti-CD34 antibody and then with FITC-labeled secondary antibody. All the sections were stained with DAPI and imaged by CLSM (LSM800, Carl Zeiss, Germany).

Preliminary toxicity of PTX with different dosages and formulations *in vivo*

To evaluate the preliminary toxicity of PTX, blood cell levels and serum biomarkers in mice were measured. Mice were randomized into 4 groups (3 mice/group): PBS, PTX-Lip (50 mg/m²), PTX-Lip (100 mg/m²), and free PTX (dissolved in ethanol-Cremophor ELP 35 mixture, v/v = 1:1,100 mg/m²). After injection of the different formulations three times, mice were euthanized and blood samples were obtained for a blood cell assay and a serum chemistry assay.

Evaluation of anti-tumor activity *in vivo*

BXPC-3 subcutaneous tumor-bearing mice were randomized into 6 groups: PBS, single agents (50 mg/m² PTX-Lip per dose, 0.35 mg/kg LH-Lip/siBCL-2 per dose), or their combinations (PTX-Lip plus N-Lip/siBCL-2, PTX-Lip plus LH-Lip/siCTL, and PTX-Lip plus LH-Lip/siBCL-2). PTX-Lip was given on day 7, day 9, and day 11, and other formulations were given on day 8, day 10 and day 12. Animal body weight and tumor volumes were monitored every 3 days. On the 22nd day, half of the mice were euthanized and their tumors were collected. The survival time of each group was continuously recorded. The expressions of BCL-2 and Caspase-3 in tumors were measured by western blotting. Tumor histology was performed after hematoxylin and eosin (H&E), BCL-2 and Caspase-3 staining. To quantify the relative BCL-2 mRNA expression in the tumor, mice were euthanized at 48 h after treatment with the different formulations. Total RNA was then harvested from tumors and qRT-PCR was performed.

A BXPC-3 metastatic tumor mouse model was established by intravenous injection of a suspension of $1×10^6$ BXPC-3 cells (100 µL) via the tail vein into 4-week-old female nude mice. Before cancer cell injection, mice were injected with PTX-Lip (50 mg/m² per dose) three times. N-Lip/siBCL-2, LH-Lip/siCTL and LH-Lip/siBCL-2 (0.35mg/kg siRNA per dose) were given on day 10 three times after cancer cell injection. Animal body weight was monitored every 3 days. On the 30th day, half of the mice were euthanized and their lungs and livers were collected and histology was performed after H&E staining. Lung histology was performed after Ki67 staining. The survival time of each group was continuously recorded.

Statistical analysis

All data are expressed as mean ± SD. Statistical comparisons were performed using one-way ANOVA for multiple groups (GraphPad Prism, V5.01, GraphPad, La Jolla, CA, USA). Two-tailed Student's t-test was used to compare two groups. Significant differences between or among groups are indicated by *$P < 0.05$, **$P < 0.01$, and ***$P < 0.001$, respectively.

Results

Characterization of lipoplex

To reduce the toxicity of cationic liposomes and improve their stability, LH-coated lipid-siRNA complex was prepared. After coating with LH (1 mg/mL), LH-Lip exhibited a negative charge and the size increased from 100 nm to 200 nm (**Figure 1A**). When the concentration of LH increased (from 1 to 4 mg/mL), the particle diameter decreased and zeta potential increased. Negatively charged LH was coated on the surface of the cationic liposomes by electrostatic attraction. More LH wrapped tightly around the cationic liposomes with increased concentration of LH, so the size of the lipoplex gradually decreased until it was stable at around 110 nm. At the same time, the zeta potential of the lipoplex increased, which might be due to the

addition of LH changing the electrostatic repulsion between particles. To take advantage of the enhanced permeability and retention (EPR) effect, the diameters of nanoparticles should be smaller than about 150 nm [16]. In addition, too much negative charge from LH could block delivery of siRNA [17]. Therefore, we chose a relatively small diameter of LH-Lip/siBCL-2 as the optimal formulation. 8 mg/mL was chosen as the appropriate concentration of LH for preparing LH-Lip with a zeta potential of -31.20 ± 0.85 mV. The size of LH-Lip was 111.7 ± 0.99 nm, slightly larger than that of the uncoated liposomes (N-Lip) (**Figure 1B**). LH-Lip displayed an approximately spherical shape (**Figure 1C**). The binding efficiency of LH was around 50% with no significant change within 24 h (**Figure S1**). The results of agarose gel electrophoresis showed that siRNA could be absolutely loaded onto N-Lip at charge ratios (N/P) greater than 1/1 (**Figure S2**), and the siRNA encapsulation efficiencies of both lipoplexes were greater than 95% (N-Lip/Cy5-siRNA, 97.04% ± 0.00%; LH-Lip/Cy5-siRNA, 98.02% ± 0.00%).

The size of PTX-Lip was 98.23 ± 2.3 nm, and the zeta potential of PTX-Lip was -5.08 ± 0.23 mV. The drug-loading efficiency of PTX was 77.67% ± 0.02%, and the drug-loading content of PTX was 2.49 ± 0.00%. **Figure S3** shows that PTX-Lip exhibits sustained release of PTX compared to free PTX from dialysis tubes to the release media, accompanied with long blood circulation and more accumulation in the tumor (**Figure S4**).

Stability of lipoplex *in vitro*

Figure 1D shows that LH-Lip/siCTL retards siRNA degradation in serum condition, but free siCTL or free siCTL plus free LH degrade after 60 min, suggesting that LH-Lip/siCTL complex protects siRNA from degradation by serum nucleases. Although free siRNA released siRNA faster from dialysis tubes to the release media (**Figure S3**), LH-Lip/siRNA protected siRNA against degradation.

Cationic liposomes can adsorb a variety of plasma proteins in the blood leading to decreased stability [18], so the lipoplex was incubated with fetal bovine serum (FBS) and mouse serum. No obvious changes to N-Lip/siBCL-2 and LH-Lip/siBCL-2 were observed 30 min after incubation with FBS (**Figure 1E**). After incubation with mouse serum, aggregation of N-Lip/siBCL-2 was observed accompanied by an increase in size (**Figure 1F**), but no obvious change was observed for LH-Lip/siBCL-2. The size of N-Lip/siBCL-2 was greater than that of LH-Lip/siBCL-2, indicating that coating with LH prevented adsorption of serum proteins and liposome aggregation.
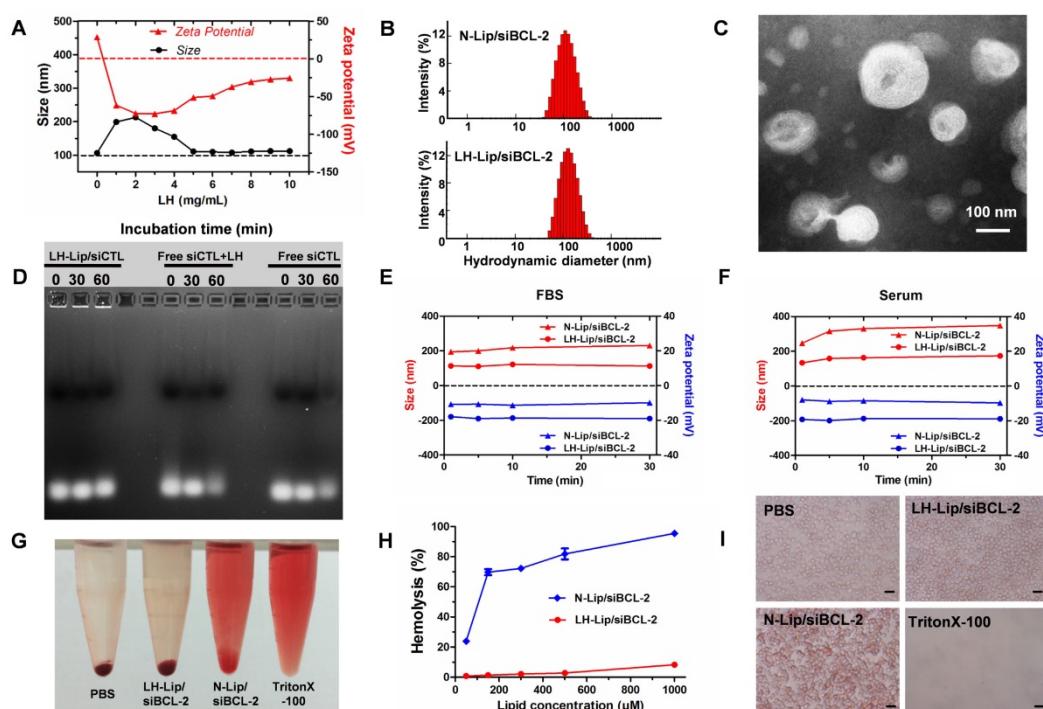

Figure 1. (A) Variation in size and zeta potential of LH-Lip/siBCL-2 with different concentrations (0-10 mg/mL) of LH. **(B)** Hydrodynamic size of N-Lip/siBCL-2 and LH-Lip/siBCL-2. **(C)** TEM image of LH-Lip/siBCL-2. Scale bar, 100 nm. **(D)** Protection of siRNA against serum nuclease degradation. LH-coated Lipid–siCTL complex, free siCTL plus free LH, and free siCTL (25 µg/mL siRNA) were respectively incubated in 50% FBS for different times (0 min, 30 min, and 60 min), and analyzed by agarose gel electrophoresis. Variation in size and zeta potential of LH-Lip/siBCL-2 and N-Lip/siBCL-2 incubated in **(E)** FBS or **(F)** mouse serum. **(G)** Photograph of Eppendrof tubes containing red blood cells treated with different formulations at a lipid concentration of 300 µM. **(H)** Hemolysis rate (%) of red blood cells treated with different concentrations of LH-Lip/siBCL-2 and N-Lip/siBCL-2. **(I)** Microscopy images of erythrocytes treated with different formulations at a lipid concentration of 300 µM. Scale bar, 15 µm.

Hemolysis assay is often used to evaluate the toxicity and safety of materials [19]. The final lipid concentration of lipoplex was 300 μM. The hemolysis rate of LH-Lip/siBCL-2 at this concentration was lower than 5% and the structure of erythrocytes was little changed. However, the hemolysis rate of N-Lip/siBCL-2 was higher than 60% at this concentration (**Figure 1G-I**).

Cellular uptake

Flow cytometry of pancreatic cancer BXPC-3 cells showed that pretreatment with PTX-Lip increased cellular uptake of LH-Lip/siBCL-2, but did not significantly enhance N-Lip/siBCL-2 uptake (**Figure 2A-B**). This might be because cationic liposomes are easily internalized and pretreatment with PTX-Lip had little effect on their uptake. The cellular uptake of LH-Lip/siBCL-2 increased with increasing PTX concentration (0-1 μg/mL) and reached a maximum at a concentration of 0.3 μg/mL (**Figure 2C**). Our previous study demonstrated that pretreatment with docetaxel promoted the uptake of nanoparticles, and

it was mainly caused by the G2/M retention effect [20]. The G2/M retention effect describes the fact that the uptake ability of cells is strongest in the G2/M phase rather than other phases [21]. The percentage of BXPC-3 cells in G2/M phase increased with increasing PTX concentration (**Figure 2D**).

Subcellular localization microscopy showed that free siRNA was minimally internalized by the cells (**Figure 2E**). However, fluorescence signal was obviously observed in the LH-Lip/siRNA group, indicating that LH-Lip/siRNA promoted uptake of siRNA into BXPC-3 cells. This enhanced uptake might result from the LH coating. Fibroblast growth factors (FGFs) have a high affinity for glycosaminoglycan heparin and promote the combination of heparin and fibroblast growth factor receptor (FGFR) [22]. The BXPC-3 cells exhibited high expression levels of FGF2 (a classical isomer of the FGF family) (**Figure S5**). In addition, the pretreatment with PTX-Lip further promoted cellular internalization of LH-Lip/siRNA (**Figure 2E**).
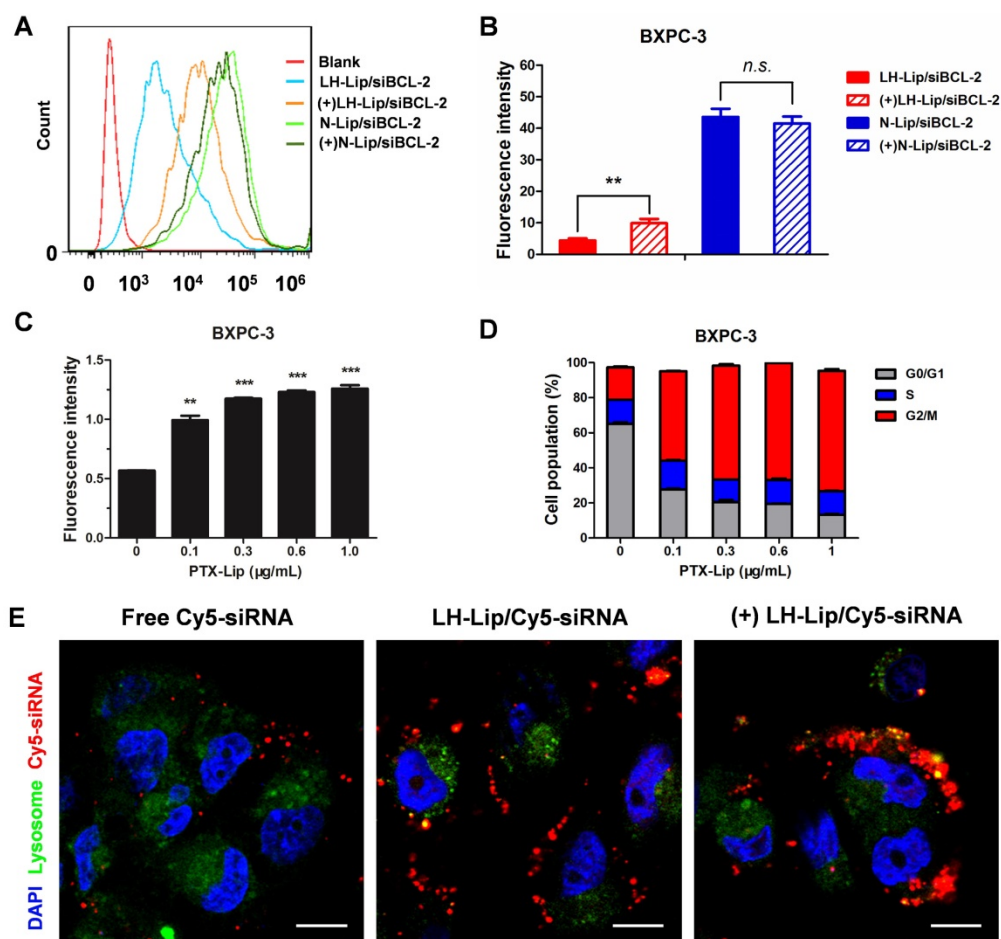

Figure 2. (A) Flow cytometry cellular uptake assay of BXPC-3 cells treated with different formulations. **(B)** Quantitative analysis of cellular uptake (n = 3). ** P < 0.01. (+) represents incubation with PTX-Lip (0.3 μg/mL) before treatment. **(C)** Cellular uptake of CFPE-labeled LH-Lip after pretreatment with PTX-Lip at different concentrations (n = 3). **P < 0.01, ***P < 0.005 vs. the group without pretreatment. **(D)** Cell cycle distribution of BXPC-3 cells treated with different concentrations of PTX-Lip (n = 3). **(E)** The intracellular distribution of Cy5-labeled siRNA in BXPC-3 cells after 2 h incubation. Nuclei were stained with DAPI (blue). Co-localization of Cy5-siRNA (red) and lysosomes (green) is displayed as yellow fluorescence. Scale bar, 10 μm.

Silencing effect of siBCL-2-loaded liposomes on BCL-2 and cytochrome C expression

FITC-labeled rabbit anti-human BCL-2 was used to detect BCL-2 expression. The pretreatment with PTX-Lip significantly increased the expression of BCL-2 (**Figure 3A**). LH-Lip/siBCL-2 significantly inhibited the expression of BCL-2 induced by chemotherapeutics, while N-Lip/siBCL-2 slightly inhibited BCL-2 levels (**Figure 3B-C**). This might be because N-Lip induced high levels of apoptosis (**Figure 3F**), and expression of BCL-2 is closely related to apoptosis [7]. To investigate the relationship between concentration of siBCL-2 and silencing efficiency, BXPC-3 cells were treated with different concentrations of siBCL-2-loaded LH-Lip, and BCL-2 mRNA was measured using qRT-PCR. The result showed that the pretreatment with PTX-Lip significantly increased the BCL-2 mRNA level, and LH-Lip/siBCL-2 reduced the BCL-2 mRNA level in a dose-dependent manner (**Figure S6**). The siBCL-2 concentration that produced 50% inhibition was about 50 nM, so we chose this concentration for the further studies.

BCL-2 exerts anti-apoptotic effects by preventing release of mitochondrial cytochrome C [23].

Therefore, the expression levels of cytochrome C in mitochondria and cytoplasm could further demonstrate the silencing effect of siBCL-2. **Figure 3D** shows that PTX-Lip induces higher cytochrome C levels in mitochondria. However, LH-Lip/siBCL-2 inhibited the cytochrome C levels in mitochondria and showed approximately the same levels in the cytoplasm as control.

Cellular apoptosis assay and cytotoxicity study

Apoptosis induced by the different lipoplexes was measured using an Annexin V-FITC/PI Apoptosis Detection Kit. LH-Lip/siBCL-2 induced significantly less apoptosis and necrosis in LO2 cells (**Figure 3E** and **Figure S7**) but significantly more BXPC-3 cell necrosis (**Figure 3F** and **Figure S8**) than did N-Lip/siBCL-2. This result might be due to the fact that the toxicity of free LH to BXPC-3 cells was significantly greater than that to LO2 cells (**Figure 3G-H**). On the other hand, the anti-proliferation effect was enhanced with the increasing PTX concentration, and the LH-Lip/siBCL-2 group showed much lower cell viability compared to the other groups (**Figure 3I**).
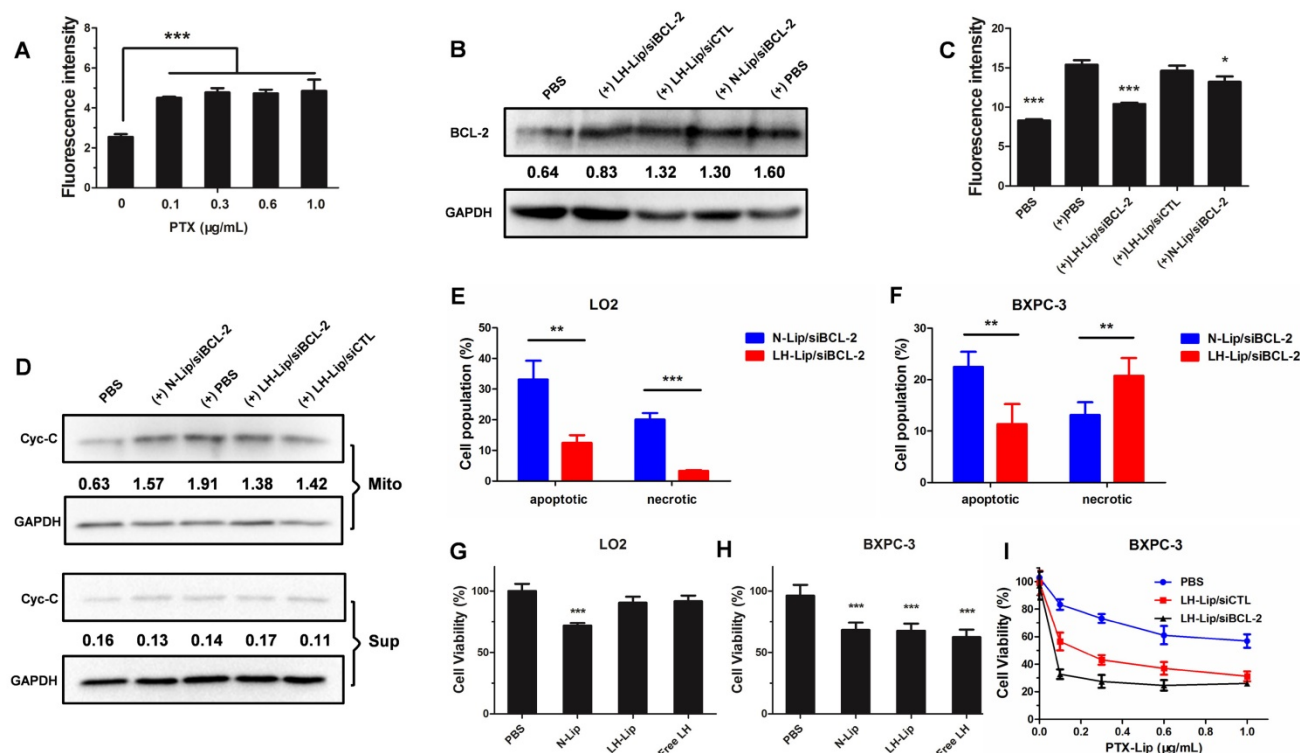

Figure 3. (A) The expression of BCL-2 on BXPC-3 cells after pretreatment with PTX-Lip at different concentrations (n = 3). **(B)** The expression levels of BCL-2 and GAPDH on BXPC-3 cells after treatment with different formulations (measured by western blotting). (+) represents incubation with PTX-Lip (0.3 μg/mL) before treatment. The numbers shown with the western blots represent the gray values normalized to GAPDH. **(C)** The expression of BCL-2 on BXPC-3 cells after treatment with different formulations (n = 3). *P < 0.05, **P < 0.01, ***P < 0.005 vs. the (+) PBS group. **(D)** The expression levels of cytochrome C (Cyc-C) in the mitochondria and cytoplasm of BXPC-3 cells after treatment with different formulations (measured by western blotting). Mito: mitochondria; Sup: cytoplasm. The percentage of apoptotic and necrotic **(E)** LO2 and **(F)** BXPC-3 cells (n = 3). **P < 0.01, ***P < 0.005. The cytotoxicity of the different lipoplexes to **(G)** LO2 and **(H)** BXPC-3 cells (n = 5). **P < 0.01, ***P < 0.005 vs. the PBS group. **(I)** The cytotoxicity of different formulations to BXPC-3 cells after pretreatment with PTX-Lip at different concentrations (n = 5).

Effects of tumor priming

Three-dimensional tumor spheroids were prepared to evaluate the solid tumor penetration ability of the lipoplex after tumor priming. The results showed that tumor spheroid uptake increased at different depths with increasing PTX concentration and reached a maximum at a concentration of 0.3 μg/mL (**Figure 4A**). Additionally, the penetration ability of Cy5-labeled siRNA was also enhanced after priming with PTX-Lip (**Figure S9**). Compared to other tumors, PDAC is rich in ECM components, such as collagen I, hyaluronic acids and cancer-associated fibroblasts, which hinder the delivery of nanoparticles [24-26]. Transwell chambers were used to evaluate penetration of a tumor stroma barrier composed of fibroblasts. In the upper chamber, cellular uptake by NIH-3T3 cells (**Figure 4B**) was the same as that shown in **Figure 2B**. In the lower chamber, cellular uptake of the lipoplex by BXPC-3 cells was significantly increased with pretreatment compared to the non-pretreated group (**Figure 4C**), indicating that tumor priming could increase the penetration ability of lipoplex through fibroblasts.

BXPC-3 subcutaneous tumor-bearing nude mice were used to estimate tumor penetration with tumor priming *in vivo*. The pretreatment with PTX increased the penetration of DID-labeled LH-Lip compared to the PBS group (**Figure 5A-B** and **Figure S10**), and stronger fluorescence was observed with pretreatment for 24 h vs. 48 h (**Figure 5C**). After injection of PTX-Lip at 50 mg/m^2 for 24 h, the penetration ability of Evans Blue in tumor tissues was enhanced by 63% compared to the free PBS group, and was stronger than that of the free PTX group (**Figure 5D**). Additionally, there were no significant differences in penetration ability between groups pretreated with PTX-Lip at the doses 50 mg/m^2 and 100 mg/m^2. Therefore, pre-injection of PTX-Lip at 50 mg/m^2 for 24 h was selected for further study. Immuno-histo-chemical images showed that the pretreatment with PTX-Lip increased cell apoptosis in the tumor, but decreased the expression of α-SMA and collagenous fibers (**Figure S11**), which are components of tumor stroma [27].
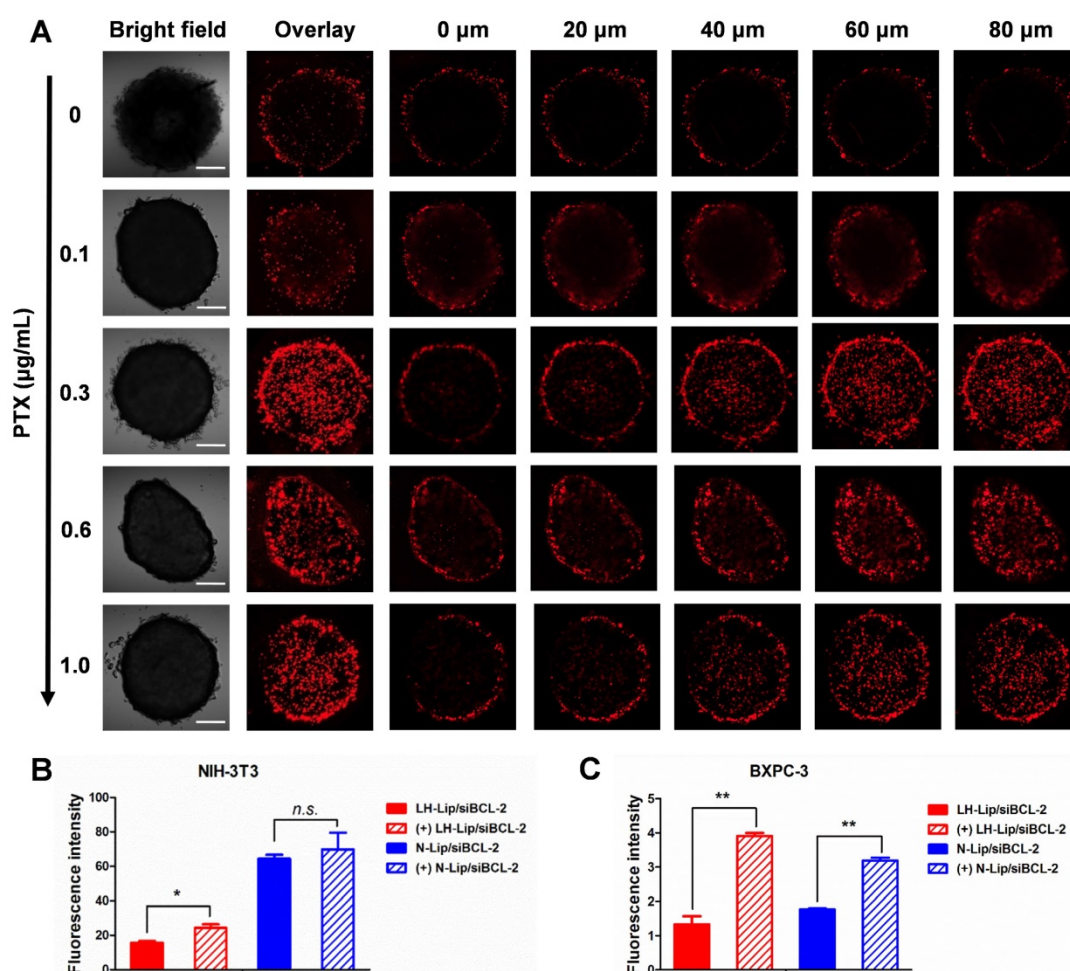

Figure 4. (A) Tumor spheroids uptake after pretreatment with PTX-Lip at different concentrations. Scale bar, 100 μm. Cellular uptake of lipoplex in **(B)** NIH-3T3 cells (upper) and **(C)** BXPC-3 cells (lower) in a Transwell *in vitro* model (n = 3). *P < 0.05, **P < 0.01.
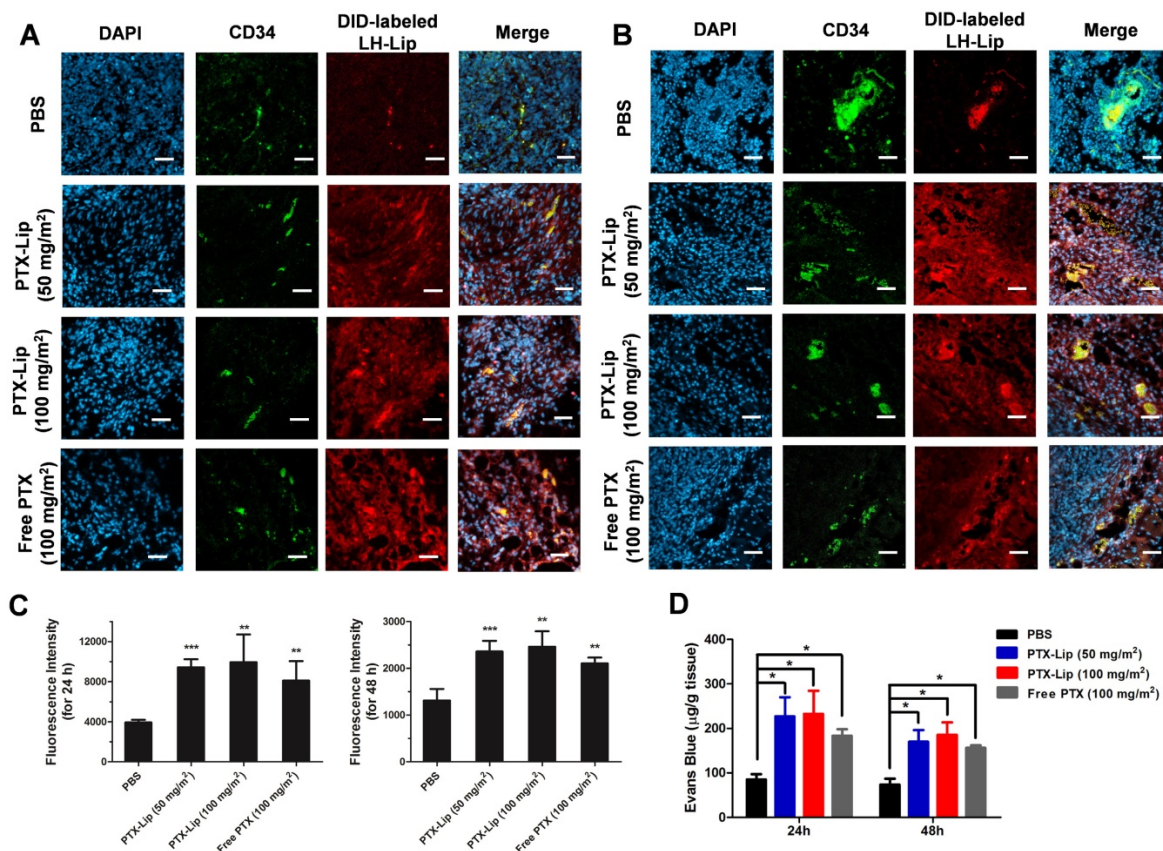
Figure 5. Penetration of LH-Lip into tumor tissue **(A)** 24 h or **(B)** 48 h after pretreatment with different PTX formulations. Blue, green and red represent nuclei, CD34 staining and DID-labeled LH-Lip, respectively. Scale bar, 50 μm. **(C)** Quantitation of the CLSM images. **(D)** Evans Blue dye penetration into tumors (n = 3). *P < 0.05, **P < 0.01, *** P <0.005 vs. the PBS group.

Preliminary toxicity of PTX with different dosages and formulations *in vivo*

A previous study demonstrated that pretreatment with free PTX could promote the interstitial transport, penetration and dispersion of nanoparticles [6]. However, free PTX causes severe myelosuppression, and Cremophor induces anaphylaxis [28]. PTX liposomes can avoid Cremophor as a solvent and can reduce the therapeutic dose and toxicity of PTX. **Table 1** shows that mice treated with free PTX (100 mg/m²) displayed a significant decrease in white blood cells (WBC), platelets (PLT) and neutrophile granulocyte (Gran) compared to the PBS group, indicating severe myelosuppression of the blood system. No significant differences in WBC, PLT and Gran were observed between mice treated with PTX-Lip (50 mg/m²) and PBS.

Glutamic-pyruvic transaminase (ALT) and alkaline phosphatase (ALP) are measured to monitor hepatic function [29], and urea nitrogen (BUN) and creatinine (CREA) are measured to assess renal function [30]. **Table 2** indicates that the level of ALT and ALP significantly increased in the free PTX (100 mg/m²) group and the PTX-Lip (100 mg/m²) group, but changes in the PTX-Lip (50 mg/m²) group were

negligible. Additionally, no obvious influence on BUN and CREA was observed among all groups. Therefore, a low dose (50 mg/m²) of PTX-Lip showed lower toxicity than a higher dose (100 mg/m²) of PTX-Lip and free PTX.

Table 1. Blood cell levels in mice after treatment with different PTX formulations (n = 3).

Groups	WBC (10^9/L)	PLT (10^9/L)	Gran (10^9/L)
PBS	3.63 ± 0.25	398.3 ± 15.0	1.57 ± 0.15
PTX-Lip (50 mg/m²)	3.67 ± 0.15	366.3 ± 15.0	1.37 ± 0.32
PTX-Lip (100 mg/m²)	3.50 ± 0.10	282.7 ± 11.8*	1.20 ± 0.20
Free PTX (100 mg/m²)	0.97 ± 0.35*	250.0 ± 9.54*	0.43 ± 0.15*

WBC: white blood cells; PLT: platelets; Gran: neutrophile granulocyte.
*P < 0.001 vs. PBS group.

Table 2. Serum biomarkers in mice after treatment with different PTX formulations (n = 3).

Groups	ALT (U/L)	ALP (U/L)	BUN (mM)	CRE (μM)
PBS	42.25 ± 4.03	114.1 ± 12.0	6.78 ± 0.35	34.5 ± 2.12
PTX-Lip (50 mg/m²)	40.05 ± 4.17	106.3 ± 16.3	6.80 ± 0.67	37.0 ± 2.83
PTX-Lip (100 mg/m²)	114.2 ± 4.88**	140.8 ± 9.69*	6.46 ± 0.71	32.3 ± 3.18
Free PTX (100 mg/m²)	369.8 ± 3.11***	191.5 ± 16.3*	6.66 ± 0.96	34.5 ± 2.12

ALT: glutamic-pyruvic transaminase; ALP: alkaline phosphatase; BUN: urea nitrogen; CRE: creatinine.
*P < 0.05, **P < 0.01, and ***P < 0.001 vs. PBS group.

Inhibitory effect on cell migration and invasion

A previous study demonstrated the inhibitory effect of LH on melanoma cell migration and invasion [14]. Here, wound healing assay was used to evaluate the migration of BXPC-3 cells. Both LH-Lip/siBCL-2 and pretreated groups hindered the migration of BXPC-3 cells, and the combination of pretreatment and LH-Lip/siBCL-2 exhibited the strongest inhibitory effect (**Figure 6A** and **Figure S12**). N-Lip/siBCL-2 also hindered cell migration, attributed to the anti-metastatic effect of siBCL-2 [9]. Matrigel-coated transwell chambers were used to evaluate cell invasion. As shown in **Figure 6B** and **Figure S13**, BXPC-3 cells were aggressive and could easily penetrate the matrigel layer. The combination of pretreatment and LH-Lip/siBCL-2 exhibited the strongest inhibitory effect.

Interactions of tumor cells with platelets and actin cytoskeleton

Emerging evidence indicates that platelets promote cancer metastasis via platelet–tumor cell interactions, and induce an epithelial-mesenchymal-like transition (EMT) [31]. A previous study demonstrated that LH could inhibit the adhesion of platelets and melanoma cells [14], but its inhibitory effect on pancreatic cancer cells has not been evaluated. The results of this study suggested that formulations with LH could significantly inhibit the adhesion of platelets and BXPC-3 cells (**Figure 6C** and **Figure S14**). EMT is pivotal for metastasis of PDAC [32], and the switch between E- and N-cadherin is a classical feature of EMT [33]. After incubation with platelets, the expression of E-cadherin decreased but N-cadherin levels increased, indicating that platelets could induce EMT of BXPC-3 cells. However, BXPC-3 cells treated with the formulation with LH expressed more E-cadherin and less N-cadherin (**Figure 6D**). The tensile forces of actin stress fibers encourage tumor cells to invade and metastasize [34]. CLSM imaging indicated that formulations with LH attenuated the formation of actin filaments and lamellipodia (**Figure 6E**).

Anti-tumor and anti-metastasis efficacy

BXPC-3 subcutaneous tumor-bearing mice were injected with free Cy5-siRNA and Cy5-siRNA-loaded liposomes. In the tumor, a higher fluorescence signal was observed in the LH-Lip/Cy5-siRNA group than in the free Cy5-siRNA group (**Figure S15**). This is logical because the LH-coated lipoplex should have prolonged circulation compared to cationic liposomes [35]. Additionally, the pretreatment with PTX-Lip increased the tumor penetration of Cy5-siRNA compared to the un-pretreated group. The tumor-to-liver ratio of LH-Lip/Cy5-siRNA was highest among all groups (**Figure S16**). This suggested that LH-Lip/Cy5-siRNA exhibited better behavior *in vivo*, with more tumor accumulation and relatively less distribution to the liver than the other formulations.

For evaluating the therapeutic effect, mice were treated as shown in **Figure 7A**. Malignant tumor always increases body energy consumption, resulting in body weight loss [36]. However, body weight increased gradually during the treatment (**Figure 7B**), which might be caused by rapid increases in tumor weight during the early stage of tumorigenesis. Treatment with LH-Lip/siBCL-2 alone did not significantly prolong the survival time (27 days), but pretreatment with a low dose of PTX-Lip before administration of LH-Lip/siBCL-2 significantly prolonged the survival time to 39 days (**Figure 7C**). The pretreatment with PTX-Lip before administration of nanodrugs (including LH-Lip/siBCL-2, LH-Lip/siCTL, and N-Lip/siBCL-2) also showed significant reduction in tumor growth (**Figure 7D-F**). The expressions of BCL-2 and Caspase-3 were detected using western blotting and immuno-histochemical staining. **Figure 7H** shows that treating with PTX-Lip induced high BCL-2 levels in tumor tissues, but the combination with siBCL-2 reduced the expression of BCL-2, indicating that the dramatic silencing effect of siBCL-2-loaded liposomes. The relative expression levels of BCL-2 mRNA (**Figure 7G**) showed the same result as western blotting. Additionally, PTX-Lip in combination with LH-Lip/siBCL-2 induced significant apoptosis according to the apoptosis marker Caspase-3 (**Figure 7H-I**).

A previous study demonstrated that free PTX exacerbates cancer metastasis [5], which is a risk factor for chemotherapy. To test whether PTX-Lip affects cancer metastasis, mice were treated following the scheme presented in **Figure 8A**. Mice showed continuous weight loss from day 18, which was obvious in the PBS and PTX-Lip treatment groups (**Figure 8B**). No change in survival time was observed in groups treated with PBS or PTX-Lip alone (**Figure 8C**). Metastatic nodules in the lungs and liver significantly increased in the PTX-Lip-treated group (**Figure 8E-G**), indicating that pretreatment with PTX-Lip exacerbated pancreatic cancer metastasis. However, our ideal formulation could reduce the risk of cancer metastasis and prolong the survival time. H&E-stained images of lungs show that this combination therapeutic strategy inhibited edema in the parenchyma (**Figure 8D**), resulting in inhibition of the inflammatory response. Additionally, Ki67-stained images of lungs show active cell proliferation activity in metastatic nodules (**Figure S17**).
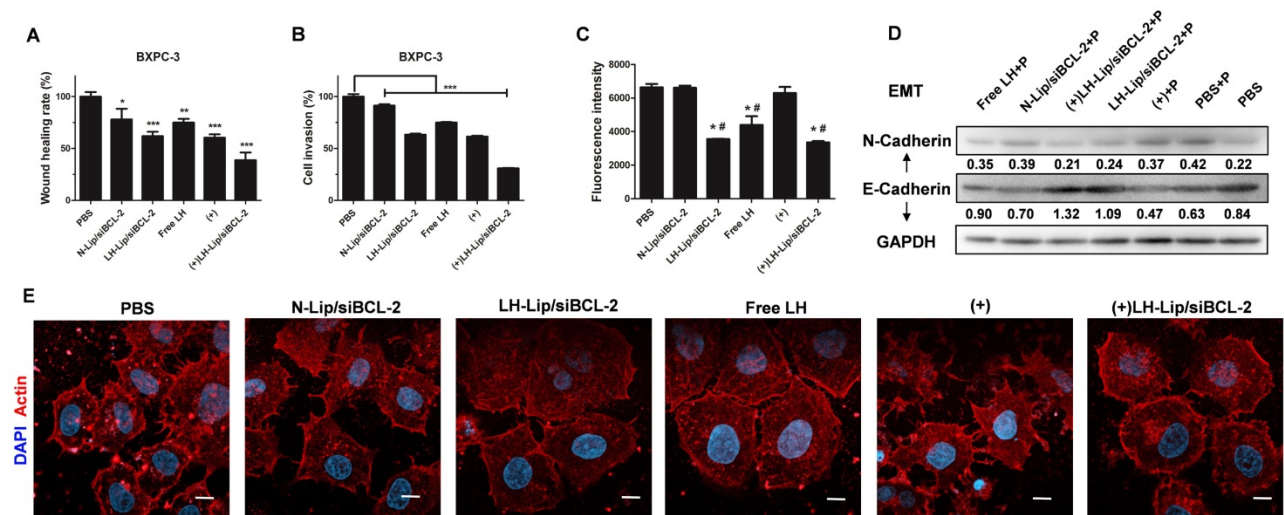
Figure 6. (A) Wound healing assay and **(B)** cell invasion assay (n=3). *P < 0.05, **P < 0.01, ***P < 0.005 vs. the PBS group. **(C)** Effects of different formulations on tumor cell−platelet interactions. *P < 0.005 vs. the PBS group; #P < 0.005 vs. the (+) group. **(D)** The expression levels of N-Cadherin and E-Cadherin. P: platelets. The numbers shown with the western blots represent the gray value normalized to GAPDH. **(E)** Actin cytoskeleton of BXPC-3 cells. Scale bar, 10 µm. (+) represents incubation with PTX-Lip (0.3 µg/mL) before treatment.
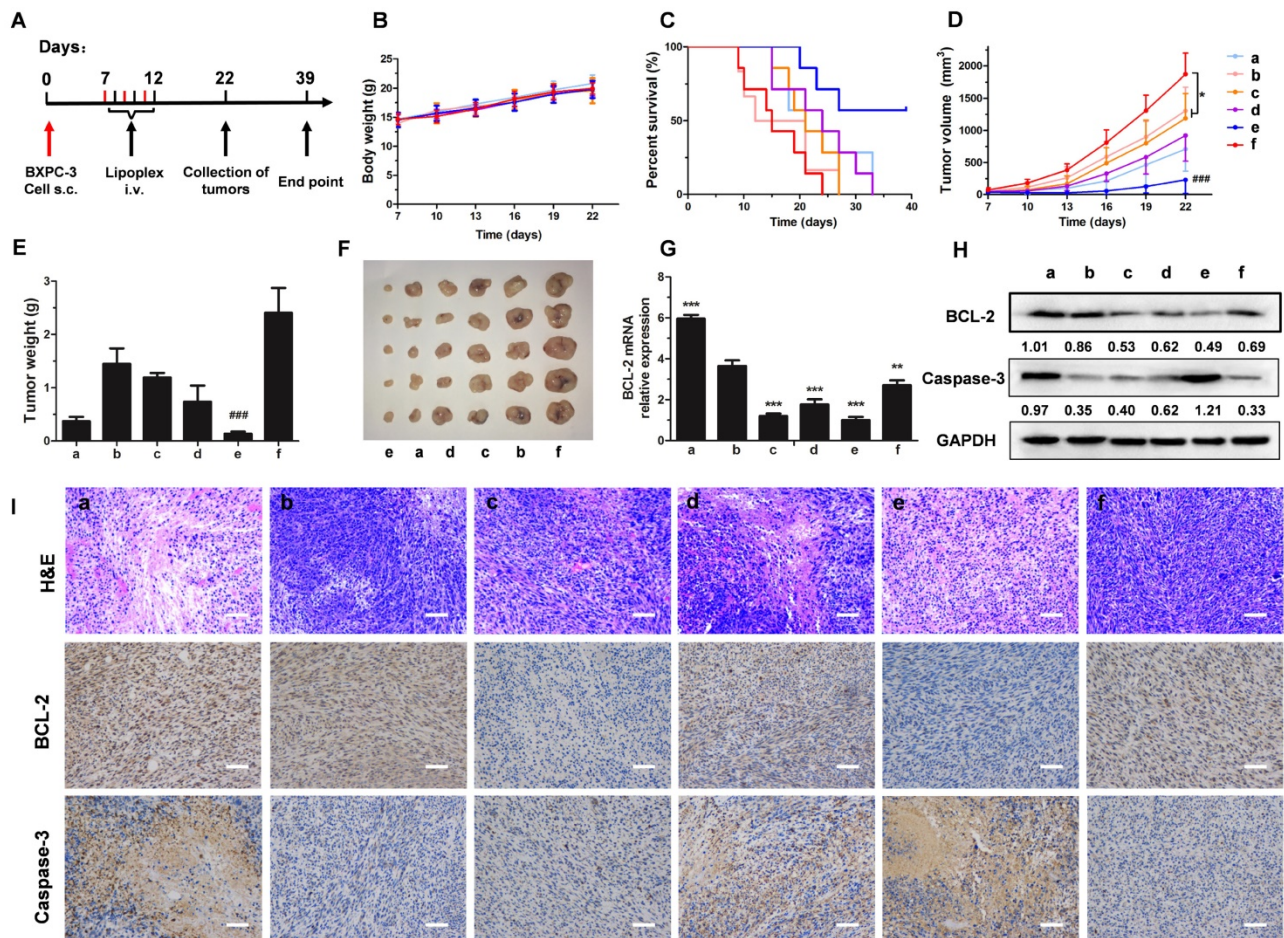

Figure 7. (A) The experimental scheme. **(B)** The body weights of mice during the treatment (n = 6). **(C)** Kaplan-Meier survival curve of mice (n = 7). **(D)** The tumor growth curves and **(E)** tumor weights of mice (n = 6). *P < 0.05 vs. PBS group, ###P < 0.001 vs. other groups. **(F)** Representative photographs of tumors at the end of the treatment procedure. **(G)** The expression levels of BCL-2 mRNA in tumor tissues at 48 h after treatment with different formulations (n = 3). **P < 0.01, ***P < 0.005 vs. (+) PBS group. **(H)** The expression levels of BCL-2 and Caspase-3 in tumor tissues by western blotting. The numbers shown with the western blots represent the gray value normalized to GAPDH. **(I)** H&E staining, BCL-2 staining and Caspase-3 staining of tumor tissues (positive cells shown in brown). Scale bar, 100 µm. a = (+) LH-Lip/siCTL, b = (+) PBS, c = LH-Lip/siBCL-2, d = (+) N-Lip/siBCL-2, e = (+) LH-Lip/siBCL-2, f = PBS. (+) represents injection of PTX-Lip (50 mg/m²) before treatment.
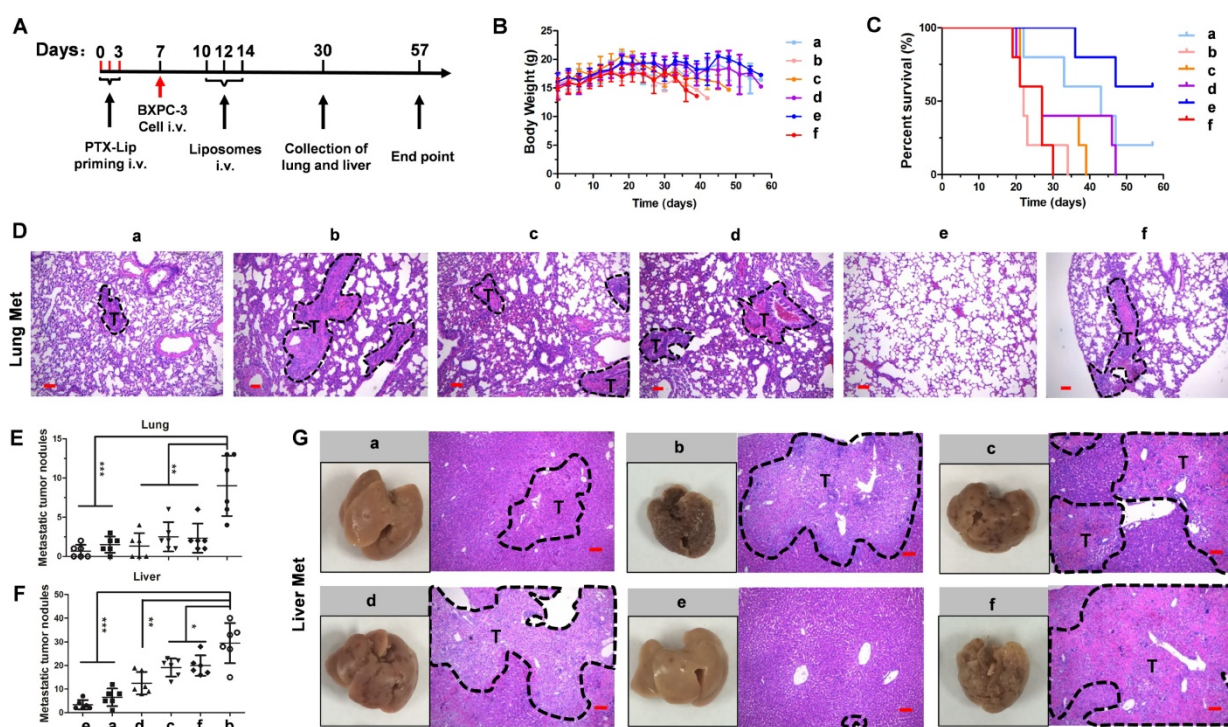
Figure 8. (A) The experimental scheme. **(B)** The body weights of mice during the treatment (n = 5). **(C)** Kaplan-Meier survival curves of mice (n = 5). **(D)** H&E staining of lungs. Number of metastatic nodules in the **(E)** lung or **(F)** liver (n = 5). *P < 0.05, **P < 0.01, ***P < 0.005 vs. the (+) PBS group. **(G)** Representative photographs of livers and H&E staining of livers at the end of the treatment procedure. Dashed lines, metastatic loci. Scale bar, 100 μm. a = (+) LH-Lip/siCTL, b = (+) PBS, c = LH-Lip/siBCL-2, d = (+) N-Lip/siBCL-2, e = (+) LH-Lip/siBCL-2, f = PBS. (+) represents injection of PTX-Lip (50 mg/m²) before treatment.

Discussion

Cationic liposomes are widely used in gene delivery, but they change the cell membrane potential and induce cytotoxicity by rupturing the membrane [37]. When cationic liposomes enter the blood circulation, they bond with negatively charged plasma protein in the blood, resulting in aggregation and sedimentation [18]. All these adverse factors impede the clinical application of cationic liposomes. In our study, the combination of LH and cationic liposomes made the surface potential of the carrier switch from positive to negative (**Figure 1A**), thus significantly reducing aggregation and precipitation (**Figure 1E-F**). Cationic liposomes, N-Lip, obliviously caused rapid red blood cell rupture. However, LH-coated lipoplex exhibited little hemolytic toxicity at the same concentration range (**Figure 1 H**). Additionally, LH-Lip significantly reduced the cell apoptosis and necrosis of normal LO2 cells caused by N-Lip (**Figure 3E**). The combination of LH and cationic liposomes to form a lipoplex was through electrostatic interactions, which are unstable compared to chemical bonds but require a simple preparation process. The outer LH is easily removed or degraded by heparanase [38], minimizing obstruction of siRNA transfection. BCL-2 silencing results showed that LH-Lip/siBCL-2 effectively transferred siRNA to BXPC-3 cells (**Figure 3B-C**) and tumor tissues (**Figure 7G-H**).

Pancreatic tumor always contains multiple ECM components, which impede the penetration of nanodrugs [39]. In our study, tumor priming was used to improve the tumor microenvironment, by inducing tumor cell apoptosis and decreasing the abundance of ECM (**Figure S11**). Tumor priming through PTX-Lip promoted the cellular uptake (**Figure 2C**) and delivery (**Figure 4** and **Figure 5**) of nanoparticles. Compared to free PTX, PTX-Lip exhibited lower toxicity (**Table 1** and **Table 2**) and the same penetration effect on solid tumor (**Figure 5**) at a lower dosage (50 mg/m²).

However, pretreatment with PTX may increase drug resistance or exacerbate cancer metastasis. Drug resistance is regulated via various signaling pathways. The anti-apoptotic protein BCL-2 is overexpressed in PDAC and is related to acquired chemotherapy resistance [40]. After pretreatment with PTX-Lip, the expression of BCL-2 increased (**Figure 3C** and **Figure 7G**). However, blockade of BCL-2 activity using siBCL-2 decreased this overexpression and promoted the therapeutic effect of PTX (**Figure 3I** and **Figure 7**). On the other hand, silencing BCL-2 also played a role in inhibiting cancer cell invasion and metastasis, but this anti-metastasis effect was weak using N-Lip/siBCL-2.

A previous study demonstrated that LH exhibits anti-metastasis activity to melanoma [14]. Similarly, LH-coated lipoplex also exhibited obvious anti-metastasis ability to pancreatic cancer in our study. Interestingly, PTX-Lip alone also inhibited cell migration and invasion *in vitro* because PTX-induced cytotoxicity reduced cell viability. The combination of PTX-Lip and LH-Lip/siBCL-2 obviously inhibited BXPC-3 cell migration and invasion (**Figure 6A-B**). Furthermore, the adhesion between BXPC-3 cells and platelets was inhibited using LH-Lip/siBCL-2, resulting in inhibition of the EMT process (**Figure 6C-D**). In addition, LH-Lip/siBCL-2 effectively reduced the formation of cancer metastases *in vivo* (**Figure 8**).

Conclusion

In summary, considering the specific tumor microenvironment of PDAC, we developed a novel therapeutic strategy to enhance anti-cancer and anti-metastasis efficacy. First, PTX-Lip was used as a tumor-priming agent to induce tumor cell apoptosis and decrease the abundance of ECM, resulting in enhanced the delivery of lipid-siRNA complex. Additionally, PTX-Lip showed lower toxicity and the same penetration effect on solid tumor at a lower dosage (50 mg/m²). Then, we further designed a LH-coated lipid-siRNA complex to load BCL-2 siRNA (LH-Lip/siBCL-2). This LH-coated lipoplex could not only reduce the cytotoxicity and poor stability of the cationic carriers, but also inhibit cancer metastasis *in vivo*. Sequential delivery of PTX-Lip and LH-Lip/siBCL-2 is a promising therapeutic approach for PDAC or other tumors with rich ECM and high metastatic ability.

Abbreviations

ALP: alkaline phosphatase; ALT: glutamic-pyruvic transaminase; α-SMA: alpha smooth muscle actin; BCL-2: B-cell lymphoma-2 protein; BUN: urea nitrogen; CD34: hematopoietic progenitor cell antigen; CFPE: 1, 2-dioleoyl-sn-glycero-3-phospho-ethanolamine-N-(carboxyfluorescein); CREA: creatinine; DID: 1, 1-Dioctadecyl-3, 3, 3, 3-tetramethylindo-dicarbocyanine; DOTAP: 1, 2-dioleoyl-3-trimethylam-monium-propane; ECM: extracellular matrix; EMT: epithelial-mesenchymal-like transition; FBS: fetal bovine serum; FGFR: fibroblast growth factor receptor; FGFs: fibroblast growth factors; FITC: 3',6'-dihydroxy-5-isothiocyanato-3H-spiro[isobenzofu ran-1,9'-xanthen]-3-one; Gran: neutrophile granulo-cyte; LH: low-molecular-weight heparin; PBS: phosphate buffer saline; PDAC: pancreatic ductal adenocarcinoma; PLT: platelets; PTX: paclitaxel; SPC: soybean phospholipids; WBC: white blood cells.

Supplementary Material

Supplementary figures.
http://www.thno.org/v09p0355s1.pdf

Acknowledgement

Competing Interests

The authors have declared that no competing interest exists.

References

1. Wachsmann MB, Pop LM, Vitetta ES. Pancreatic ductal adenocarcinoma. J Investig Med. 2012; 60: 643-63.
2. Neesse A, Michl P, Frese KK, Feig C, Cook N, Jacobetz MA, et al. Stromal biology and therapy in pancreatic cancer. Gut. 2011; 60: 861-8.
3. Tang L, Gabrielson NP, Uckun FM, Fan TM, Cheng J. Size-dependent tumor penetration and in vivo efficacy of monodisperse drug–silica nanoconjugates. Mol Pharm. 2013; 10: 883-92.
4. Khawar IA, Kim JH, Kuh HJ. Improving drug delivery to solid tumors: priming the tumor microenvironment. J Control Release. 2015; 201: 78-89.
5. Chang YS, Jalgaonkar SP, Middleton JD, Hai T. Stress-inducible gene in the noncancer host cells contributes to chemotherapy-exacerbated breast cancer metastasis. Proc Natl Acad Sci U S A. 2017; 114: E7159-68.
6. Wang J, Lu Z, Wang J, Cui M, Yeung BZ, Cole DJ, et al. Paclitaxel tumor priming promotes delivery and transfection of intravenous lipid-siRNA in pancreatic tumors. J Control Release. 2015; 216: 103-10.
7. Correia C, Lee SH, Meng XW, Vincelette ND, Knorr KLB, Ding H, et al. Emerging understanding of bcl-2 biology: implications for neoplastic progression and treatment. Biochim Biophys Acta Mol Cell Res. 2015; 1853: 1658-71.
8. Tekedereli I, Alpay SN, Akar U, Yuca E, Rodriguez CA, Han HD, et al. Therapeutic silencing of bcl-2 by systemically administered siRNA nanotherapeutics inhibits tumor growth by autophagy and apoptosis and enhances the efficacy of chemotherapy in orthotopic xenograft models of ER (−) and ER (+) breast cancer. Mol Ther Nucleic Acids. 2013; 2: e121.
9. Um HD. Bcl-2 family proteins as regulators of cancer cell invasion and metastasis: a review focusing on mitochondrial respiration and reactive oxygen species. Oncotarget. 2016; 7: 5193-203.
10. Hattori Y, Kawakami S, Suzuki S, Yamashita F, Hashida M. Enhancement of immune responses by DNA vaccination through targeted gene delivery using mannosylated cationic liposome formulations following intravenous administration in mice. Biochem Biophys Res Commun. 2004; 317: 992-9.
11. Wei X, Shao B, He Z, Ye T, Luo M, Sang Y, et al. Cationic nanocarriers induce cell necrosis through impairment of Na+/K+-ATPase and cause subsequent inflammatory response. Cell Res. 2015; 25: 237-53.
12. Li H, Chen Y, Deng Y, Wang Y, Ke X, Ci T. Effects of surface charge of low molecular weight heparin-modified cationic liposomes on drug efficacy and toxicity. Drug Dev Ind Pharm. 2017; 43: 1163-72.
13. Yan H, Oommen OP, Yu D, Hilborn J, Qian H, Varghese OP. Chondroitin sulfate-coated DNA-nanoplexes enhance transfection efficiency by controlling plasmid release from endosomes: a new insight into modulating nonviral gene transfection. Adv Funct Mater. 2015; 25: 3907-15.
14. Mei L, Liu Y, Xia C, Zhou Y, Zhang Z, He Q. Polymer–drug nanoparticles combine doxorubicin carrier and heparin bioactivity functionalities for primary and metastatic cancer treatment. Mol Pharm. 2017; 14: 513-22.
15. Yu Q, Qiu Y, Wang X, Tang J, Liu Y, Mei L, et al. Efficient siRNA transfer to knockdown a placenta specific lncRNA using RGD-modified nano-liposome: A new preeclampsia-like mouse model. Int J Pharm. 2018; 546: 115-24.
16. Danaei M, Dehghankhold M, Ataei S, Hasanzadeh DF, Javanmard R, Dokhani A, et al. Impact of particle size and polydispersity index on the clinical applications of lipidic nanocarrier systems. Pharmaceutics. 2018; 10.
17. Ho W, Zhang XQ, Xu X. Biomaterials in siRNA delivery: a comprehensive review. Adv Healthc Mater. 2016; 5: 2715-31.
18. Semple SC, Akinc A, Chen J, Sandhu AP, Mui BL, Cho CK, et al. Rational design of cationic lipids for siRNA delivery. Nat Biotechnol. 2010; 28: 172-6.
19. Tian X, Zhu M, Du L, Wang J, Fan Z, Liu J, et al. Intrauterine inflammation increases materno-fetal transfer of gold nanoparticles in a size-dependent manner in murine pregnancy. Small. 2013; 9: 2432-9.

20. Gao H, Hu G, Zhang Q, Zhang S, Jiang X, He Q. Pretreatment with chemotherapeutics for enhanced nanoparticles accumulation in tumor: the potential role of G2 cycle retention effect. Sci Rep. 2014; 4: 4492.

21. Kim JA, Åberg C, Salvati A, Dawson KA. Role of cell cycle on the cellular uptake and dilution of nanoparticles in a cell population. Nat Nanotechnol. 2011; 7: 62-8.

22. Sperinde GV, Nugent MA. Mechanisms of fibroblast growth factor 2 intracellular processing: a kinetic analysis of the role of heparan sulfate proteoglycans. Biochemistry. 2000; 39: 3788-96.

23. An J, Chen Y, Huang Z. Critical upstream signals of cytochrome c release induced by a novel Bcl-2 inhibitor. J Biol Chem. 2004; 279: 19133-40.

24. Shields MA, Dangi-Garimella S, Redig AJ, Munshi HG. Biochemical role of the collagen-rich tumour microenvironment in pancreatic cancer progression. Biochem J. 2012; 441: 541-52.

25. Provenzano PP, Cuevas C, Chang AE, Goel VK, Von Hoff DD, Hingorani SR. Enzymatic targeting of the stroma ablates physical barriers to treatment of pancreatic ductal adenocarcinoma. Cancer Cell. 2012; 21: 418-29.

26. Pan B, Liao Q, Niu Z, Zhou L, Zhao Y. Cancer-associated fibroblasts in pancreatic adenocarcinoma. Future Oncol. 2015; 11: 2603-10.

27. Hanley CJ, Noble F, Ward M, Bullock M, Drifka C, Mellone M, et al. A subset of myofibroblastic cancer-associated fibroblasts regulate collagen fiber elongation, which is prognostic in multiple cancers. Oncotarget. 2016; 7: 6159-74.

28. Chetan N, Sharad J, Ankit S, Vaibhav K, Noor A, Ravindra Dhar D, et al. Paclitaxel formulations: challenges and novel delivery options. Curr Drug Deliv. 2014; 11: 666-86.

29. Ozer JS, Chetty R, Kenna G, Palandra J, Zhang Y, Lanevschi A, et al. Enhancing the utility of alanine aminotransferase as a reference standard biomarker for drug-induced liver injury. Regul Toxicol Pharmacol. 2010; 56: 237-46.

30. Smith GL, Shlipak MG, Havranek EP, et al. Serum urea nitrogen, creatinine, and estimators of renal function: mortality in older patients with cardiovascular disease. Arch Intern Med. 2006; 166: 1134-42.

31. Labelle M, Begum S, Hynes RO. Direct signaling between platelets and cancer cells induces an epithelial-mesenchymal-like transition and promotes metastasis. Cancer cell. 2011; 20: 576-90.

32. Castellanos JA, Merchant NB, Nagathihalli NS. Emerging targets in pancreatic cancer: epithelial–mesenchymal transition and cancer stem cells. Onco Targets Ther. 2013; 6: 1261-7.

33. Chen L, Muñoz-Antonia T, Cress WD. Trim28 contributes to EMT via regulation of E-cadherin and N-cadherin in lung cancer cell lines. PLoS One. 2014; 9: e101040.

34. Fife CM, McCarroll JA, Kavallaris M. Movers and shakers: cell cytoskeleton in cancer metastasis. Br J Pharmacol. 2014; 171: 5507-23.

35. Zhang J, Shin MC, David AE, Zhou J, Lee K, He H, et al. Long-circulating heparin-functionalized magnetic nanoparticles for potential application as a protein drug delivery platform. Mol pharm. 2013; 10: 3892-902.

36. Blum R, Kloog Y. Metabolism addiction in pancreatic cancer. Cell Death Dis. 2014; 5: e1065.

37. Wang F, Yu L, Monopoli MP, Sandin P, Mahon E, Salvati A, et al. The biomolecular corona is retained during nanoparticle uptake and protects the cells from the damage induced by cationic nanoparticles until degraded in the lysosomes. Nanomedicine. 2013; 9: 1159-68.

38. Ye T, Jiang X, Li J, Yang R, Mao Y, Li K, et al. Low molecular weight heparin mediating targeting of lymph node metastasis based on nanoliposome and enzyme–substrate interaction. Carbohydr Polym. 2015; 122: 26-38.

39. Lu H, Utama RH, Kitiyotsawat U, Babiuch K, Jiang Y, Stenzel MH. Enhanced transcellular penetration and drug delivery by crosslinked polymeric micelles into pancreatic multicellular tumor spheroids. Biomater Sci. 2015; 3: 1085-95.

40. Yang T, Xu F, Sheng Y, Zhang W, Chen Y. A targeted proteomics approach to the quantitative analysis of ERK/Bcl-2-mediated anti-apoptosis and multi-drug resistance in breast cancer. Analytical Anal Bioanal Chem. 2016; 408: 7491-503.